Biomedical Engineering Letters
https://doi.org/10.1007/s13534-019-00097-w

REVIEW ARTICLE

Current progress of photoplethysmography and SPO_2 for health monitoring

Toshiyo Tamura[1]

Received: 3 November 2018 / Revised: 5 January 2019 / Accepted: 15 January 2019

Abstract
A photoplethysmograph (PPG) is a simple medical device for monitoring blood flow and transportation of substances in the blood. It consists of a light source and a photodetector for measuring transmitted and reflected light signals. Clinically, PPGs are used to monitor the pulse rate, oxygen saturation, blood pressure, and blood vessel stiffness. Wearable unobtrusive PPG monitors are commercially available. Here, we review the principle issues and clinical applications of PPG for monitoring oxygen saturation.

Keywords Photoplethysmograph (PPG) · Pulse rate · Transmitted light · Reflected light · RGB image · Respiratory rate · Motion artifact

1 Introduction

A photoplethysmograph (PPG) is used to measure blood-flow volume and evaluate the physiological condition of a patient [1]. A PPG is a simple device consisting of a light source and detector; PPG devices that use light of different wavelengths and intensities based on light-emitting diode (LED) technology have been developed. The amount of energy transferred to the skin by light is dependent on its wavelength; for example, green light is frequently used and has a good signal-to-noise ratio (SNR) [2]. Additionally, red, green, and blue (RGB) light signals enable determination of the pulse and respiratory rates.

PPGs are typically used to determine the pulse and respiratory rates. Although PPGs can measure the rise and decline of the pulse wave, and thus provide accurate pulse-rate readings, measuring the pulse rate (PR) can be difficult in certain situations. The efficacy of other parameters, such as blood-vessel stiffness and cuffless blood pressure, has been assessed but only pulse oximetry yielded satisfactory results. Additionally, motion artifacts reduce the accuracy of continuous long-term monitoring of the PR. However, application of signal processing to remove the influence of motion artifacts yields satisfactory performance under certain conditions.

The development and applications of PPGs have been reviewed elsewhere [2–6]. Therefore, in this review, we outline the principle of PPG and the contribution of signal processing. We also describe recent developments in wearable unobtrusive PPGs, and provide an overview of effective clinical practices.

2 Photoplethysmography

2.1 Principle

The principle of PPG has been reviewed previously [2–6] and so here it is explained only briefly. Incident light traveling though skin and tissues is absorbed by, for example, pigments in the skin, bones, and arterial and venous blood. Changes in the pulsatile blood flow occur mainly in the arteries and arterioles. However, venous pulsations contribute significantly to the variability in light absorption, which influences the PPG data [7, 8]. However, we assume that this parameter does not change markedly. The volume of blood in arteries is greater during the systolic phase than the diastolic phase of the cardiac cycle. The PPG sensor optically detects changes in the pulsatile blood-flow volume (*i.e.*, changes in the detected light intensity) in the microvascular tissue bed based on the intensity of reflected and transmitted light.

✉ Toshiyo Tamura
tamurat@aoni.wadeda.jp

[1] Future Robotics Institute, Wadeda University, Tokyo, Japan

Published online: 18 February 2019

Figure 1 shows detection of a photoplethysmographic transmission waveform, which has direct current (DC) and alternating current (AC) components. The DC component of the PPG waveform corresponds to the transmitted or reflected optical signal from the tissue and depends on the structure of the tissue and the average volume of both the arterial and venous blood. The DC component changes slowly with respiration, while the AC component fluctuates according to the changes in blood volume that occur between the systolic and diastolic phases of the cardiac cycle. The fundamental frequency of the AC component depends on the heart rate (HR) and is superimposed onto the DC component.

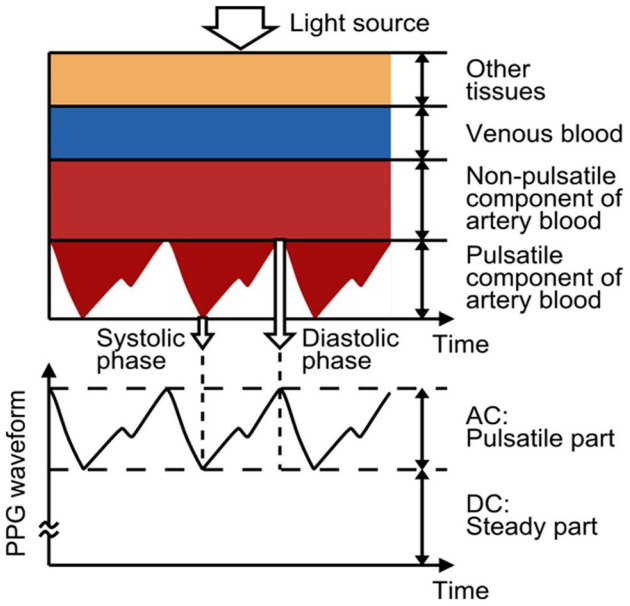

Fig. 1 Attenuation of light in tissue and blood [5]

2.2 Light source and electrical circuit

2.2.1 Light source

Light transmitted or reflected by tissue is detected by a PPG. Within the visible region, the dominant absorption peak is in the blue region of the spectrum, followed by the green-yellow region (500–600 nm), corresponding to red blood cells (Fig. 2). Light of shorter wavelengths is strongly absorbed by melanin. Water absorbs light in the ultraviolet and longer infrared (IR) regions. Red (R, 660 nm) and IR (940 nm) light passes through tissue and blood. Thus, IR light has been used in PPG sensors. In the last decade, the efficiency of LEDs has increased, and their forward voltage has decreased, resulting in an increased number of lumens per Watt. Because of high-power illumination, the cardiac cycle difference between the systolic and diastolic phases shows large variation in the green wavelength.

The absorption of green light from LEDs by oxyhemoglobin (O_2Hb) and deoxyhemoglobin (RHb) is far greater than that of IR light. Therefore, the blood-flow-induced change in the amount of reflected green light is larger than that in reflected IR light, resulting in a better SNR [9–11].

2.2.2 Sensor mode and electrical circuit

The PPG has two modes, transmission and reflectance (Fig. 3). In transmission mode, transmitted light is detected by a photodetector (PD) positioned opposite the LED, while in reflectance mode, the PD detects light backscattered or reflected from tissue, bone, and/or blood vessels.

Wearable unobtrusive PPGs use reflectance mode to enable convenient sensor placement. However, reflection-mode PPG is affected by motion artefacts and pressure disturbances. Any movement, such as physical activity, may lead to motion artefacts that corrupt the PPG signal and

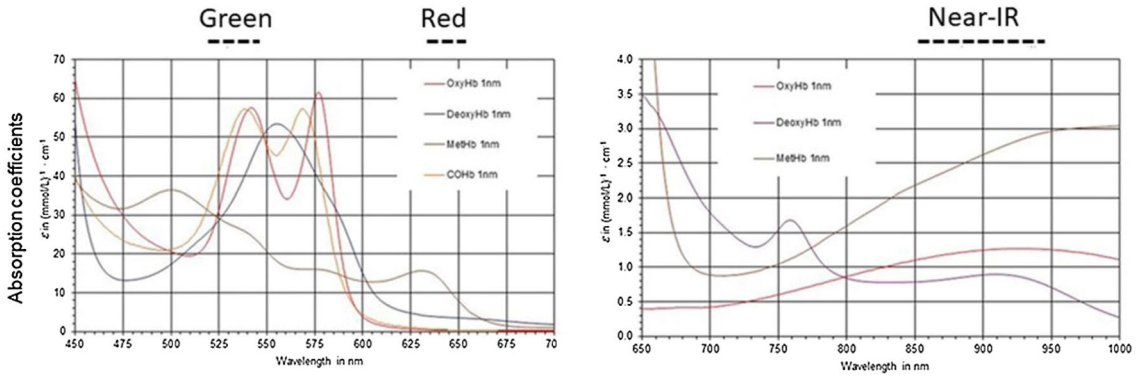

Fig. 2 Light absorption by deoxyhemoglobin (RHb), oxyhemoglobin (O_2Hb), carboxyhemoglobin (COHb), and methemoglobin (MetHb) at different wavelengths. Wavelengths of green, red and near-IR is also shown

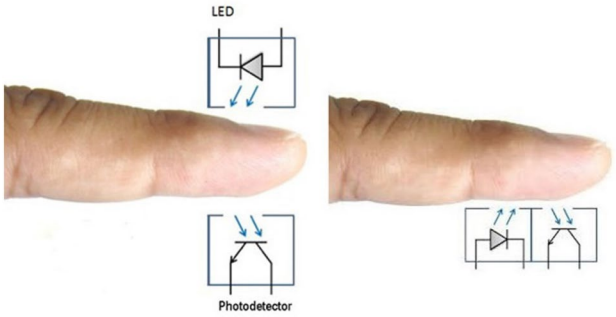

Fig. 3 Arrangement of photoplethysmograph (PPG) sensors. Left, transmission mode; right, reflectance mode

limit the measurement accuracy of physiological parameters. Pressure disturbances acting on the probe, such as the contact force between the PPG sensor and the measurement site, can deform the arterial geometry by compression (see Sect. 2.4.3). Thus, in reflectance-mode PPG, the AC amplitude may be influenced by pressure exerted on the skin.

The electrical circuit of a PPG consists of an amplifier, high-pass filter (around 0.1 Hz) to cut the DC component and obtain pulsatile signal changes, and a low-pass filter (around 30 Hz) to eliminate high-frequency noise. The frequency range used depends on the design of the circuit. The majority of wearable-type PPGs have a wireless module to enable transmission of data to a smartphone (Fig. 4a).

For mobile healthcare, a simple PPG circuit and oximeter circuit are designed and assembled because of the development of analog front-end (AFE). The AFE-based PPG consists of an analog signal conditioning circuit that uses operational amplifiers and filters, and a low-noise receiver channel with an integrated analog-to-digital converter (ADC), an LED transmit section, and diagnostics for sensor and LED fault detection. The device has a configurable timing controller. The user controls the device timing characteristics. The device communicates with an external microcontroller (Fig. 4b).

As shown in Fig. 4, the raw PPG signals are amplified and filtered, and then peaks are detected in microprocessor. The PR is calculated from intervals of the peaks. The real PPG signals are unstable, and are affected by motion artifact [12, 13]. The details on noise reduction are presented in Sect. 2.4.

2.3 Remote photoplethysmography

PPG imaging (PPGi), or remote PPG (rPPG), is a new PPG technique that involves a video camera [6] with a non-contact feature. Most recent references describe rPPGs. The principle of PR monitoring by rPPG is similar to that of reflectance-mode PPG; however, a two-dimensional (2D) image matrix is used instead of a single photodiode.

The use of an RGB video camera in rPPG has been considered, and green light provides the strongest plethysmographic signal [14–17]. Hemoglobin absorbs green light better than red light and penetrates deeper than blue light; therefore, green light yields a pulsatile signal with a marked difference between the systolic and diastolic phases. Due to its greater penetration depth than light of other wavelengths, green light is typically used for measurement of the PR and normalized pulse volume [18].

Contrasting PPG, rPPG uses ambient light and does not require a dedicated light source. Furthermore, the 2D camera sensor enables extraction of spatially separated information, which overcomes the limitation of measurements at particular locations on the skin.

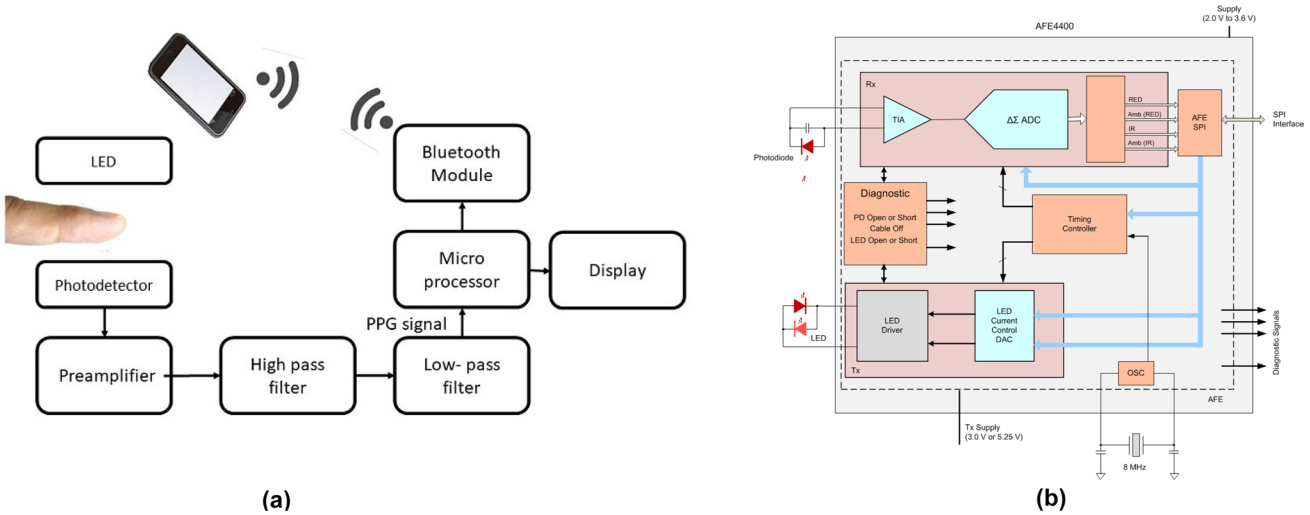

Fig. 4 Block diagram of the architecture of a PPG: **a** general circuit and **b** analog front end circuit

rPPG can be performed in noncontact mode for long distance measurements using a charge-coupled device camera to measure the light reflected from the skin. Alternatively, contact-mode rPPG, typically in conjunction with a smartphone camera, enables short-distance measurements. Plethysmographic signals can be measured using ambient light and PD with a consumer-level digital camera or smartphone. The pulse and respiratory rates are determined by processing of the RGB signal. Although the green channel has the strongest plethysmographic signal, corresponding to the absorption peak of O_2Hb, the red and blue channels also contain plethysmographic information. PPG based on ambient light with detection of multiple wavelengths (660, 810, and 940 nm) may be useful for medical applications, such as non-contact 2D reflection-mode pulse oximetry.

For skin diagnoses, an ultraviolet wavelength was added to ambient light, and devices that monitor the autofluorescence intensity and photobleaching rate show promise for detecting skin tumors [19].

2.4 Factors that affect PPG signals

PPG signals can be affected by the wavelength of light, measurement site, contact force, motion artifacts, ambient light intensity, and ambient temperature.

2.4.1 Wavelengths

Wearable PPGs typically use green light, while rPPG involves RGB signals. IR light penetrates deeper into the skin but is of low intensity and so has little pulsatile action. The penetration depth of light is dependent on its wavelength [20, 21]. The development of high-power LEDs and reflectance-mode PPG has enabled use of green light, which results in a pulsatile action far greater than that of IR light [9, 14, 22–32].

2.4.2 Measurement site

PPG sensors are commonly worn on the fingers because of the high signal amplitude that can be achieved [2]. However, this configuration is not well suited to continuous sensing because most daily activities involve use of the fingers. In recent years, various measurement sites for PPG sensors have been explored, including the ring finger [33], wrist [34, 35], brachia [11, 36, 37], in-ear [38], earlobe [39, 40], external ear cartilage [41–43], and superior auricular region [44–46]. The esophageal region has also been used in clinical practice [47–49]. Commercial clinical PPG sensors commonly use the finger, earlobe, and forehead [50]. In addition, use of a glass-type wireless PPG has been explored [51].

Wristwatch-type HR monitors and pulse oximeters have been developed and commercialized by several companies. These devices are sometimes used in clinical settings because of the feasibility of long-term use (see Sect. 2.5.2). A recently developed wristwatch-type PPG-array sensor module measures the PPG signal from the radial artery and the ulnar artery of the wrist, whereas previous devices obtained a signal from the skin capillaries. The sensitivity and accuracy of this device are enhanced by an array of phototransistors and IR-emitting diodes, and it has a conductive fiber wristband to reduce external noise [34].

2.4.3 Contact force

In reflectance-type PPG and contact rPPG, the PPG signal waveform may be affected by the contact force between the sensor and the measurement site. The waveform of the obtained PPG signal differs depending on the contact pressure of the PPG probe. The contact force applied in PPG must be carefully controlled because it exerts a strong influence on blood vessel stiffness. The optimal contact pressure corresponds to the maximal pulsatile amplitude; this occurs when the transmural pressure approaches zero (*i.e.*, under maximal arterial compliance). We also consider dynamic compliance (volume change per unit pressure change); that is, vessels are stiffer when their pressure changes quickly (*e.g.*, intrabeat) and more compliant when their pressure changes slowly. The specific slope of a photoplethysmogram-*versus*-transmural pressure curve is a function of the mechanical properties of the pulsating vessels and is sensitive to the subject's physiologic state.

Insufficient pressure results in inadequate contact and consequently a low AC signal amplitude. However, PPG signal recording under excessive pressure conditions can also lead to a low AC signal amplitude and distorted waveforms caused by the occluded artery beyond the PPG probe [52].

Despite numerous attempts, no generally accepted standards for clinical or fundamental PPG measurements of contact pressure have been adopted. Changes in the AC pulse amplitude, DC amplitude, AC: DC amplitude ratio, and normalized pulse area of the reflected PPG signal have been investigated [29, 30, 53–63]. In most experiments, the contact force is adjusted within an appropriate range using a manipulator, and the maximum AD amplitude is determined. The optimum contact pressure varies markedly among individuals due to differences in skin elasticity and blood-vessel compliance [53]. Teng and Zhang reported that the AC amplitude first increased and subsequently decreased as the contact force on the finger increased from 0.2 to 1.8 N. The AC pulse amplitude and the AC: DC amplitude ratio peaked at contact forces of 0.2 to 0.8 N due to the variation in arterial stiffness according to gender and age. In a similar contact force study, an average compression pressure of 30 mmHg (4 kPa) on the upper arm produced the maximum PPG peak amplitude for IR and green light [55].

Contact pressures of 8–12 kPa (60–90 mmHg) resulted in the largest PPG amplitude for a reflectance sensor attached to the forehead above the eye, although the SNR did not improve significantly [55]. Note that most SpO_2 studies use the ratio of the changes in R and IR light intensities (R:IR) as an accurate indicator of oxygen saturation. The R:IR values of the forehead of a newborn infant varied from 0 to 80 mmHg, and a portion of the PPG signal was derived from tissue beneath the skull [57–59].

The optimal probe-contact pressure is important, particularly for measuring arterial stiffness. Use of non-optimal probe-contact pressures results in inconsistent estimates of arterial stiffness using the PPG pulse-wave amplitude. To determine the optimal contact pressure, PPG readings were obtained in vivo from conduit artery sites in five healthy subjects using probe-contact pressures of 0–113 mmHg (0–15 kPa) [61]. The maximum amplitude was obtained at a probe-contact pressure of 95 mmHg (12 kPa). A miniaturized force regulator was designed and fabricated to adjust the PPG amplitude [63].

rPPG signals, which comprise light of three wavelengths, are also influenced by the probe-contact pressure. Light of the three wavelengths is decomposed and analyzed independently [16], but the light intensity after interaction with the biological tissue is modulated by the heartbeat frequency, mainly due to pulsatile variations in the light absorption caused by arterial blood-volume pulsations. The elastic deformations of the capillary bed are important in generating the PPG waveform. In a previously proposed PPG model, pulse oscillations of the arterial transmural pressure deform the connective-tissue components of the dermis, resulting in periodic changes in light scattering and absorption. These local changes in the light-interaction parameters are detected as variations in the light intensity reaching a camera. Therefore, arterial pulsations can be indirectly monitored using reflected light that penetrates tissue [29, 30] to determine how human skin interacts with light. Application of a glass plate to the skin modulated the temporal parameters of the light reflected from the dermis. The resulting increase in modulation amplitude of blood pulsations increased the accuracy of the pulse-rate measurement [30]. Therefore, the arterial transmural pressure must be controlled for accurate estimation of the PR by rPPG.

2.4.4 Motion artefacts

For effective PPG, motion artefacts in the low-frequency region must be eliminated. The PPG signal contains frequencies related to heart beat and respiratory function; the rest is noise. Various methods of eliminating motion artefacts have been investigated [5]. The time and frequency domain signals are processed mathematically and statistically, and motion artefacts are caused mainly by body movements. Thus, the simplest means of eliminating motion artefacts is to monitor body movements using an accelerometer and eliminate noisy signals. The skewness method, which can be used to distinguish excellent, acceptable, and poor signals, has been reported to be optimal for evaluating PPG signal quality. In this method, the Chebyshev filter improves the PPG signal quality more effectively than other digital filters [64]. A moving-average filter [65, 66] can also be used to reduce motion artefacts, but cannot adapt to sudden changes in noise (*e.g.*, due to body movements).

A Fourier series is applicable only to periodic signals; therefore, it cannot be directly applied to the nonstationary and quasiperiodic PPG signal. Generally, fast Fourier transform (FFT) analyses are followed by filter techniques [67, 68]. For, example, before FFT, a smoothing filter was used to remove high-frequency noise and then a cycle-by cycle FFT was conducted [68]. Moreover, the quasi-periodic acceleration signal is modeled using the harmonic sum (HSUM), which estimates the fundamental frequency of the acceleration signal over short periods. The fundamental frequency of the acceleration signal is then used to model the PPG signal, which contains information about the HR and motion artefacts. The HR is extracted from the PPG signal using a HSUM model [69].

Adaptive noise cancellation (ANC) using acceleration-based adaptive filters has been investigated [40, 70–86]. Identification of the optimal design usually requires a priori knowledge of certain statistical parameters (such as the mean and correlation functions) within the useful signal. With this information, an optimal filter can be designed that minimizes the unwanted signals according to statistical criteria.

Many adaptive techniques have been applied to reduce motion artefacts in PPG signals, including the normal least mean squares (NLMS) method [75–77], recursive least squares (RLS) method [78], time-varying step-size control (TVS-LMS) [79–81], adaptive step-size LMS (AS-LMS) [80], and Laguerre series [83–87].

In general, a wearable finger-type PPG device consists of a three-axis accelerometer, an IR or green LED, a photo diode, a microprocessor, and a wireless communication module. The sources of motion artefacts were investigated by computing the correlations between the three-dimensional (3D) motions and distorted PPG signals. A 2D active noise cancellation algorithm using an NLMS adaptive filter and directional accelerometer data was applied to compensate for the signal distortion [75, 76]. A NLMS filter with automatic step-size control was used to mitigate the effects of motion artefacts in PPG recordings for long-term monitoring [77].

The RLS adaptive filter recursively finds the filter coefficients that minimize a weighted linear least squares cost function related to the input signal. A fast transversal RLS algorithm was applied to reduce the computational

complexity of the adaptive filter by providing an estimate of the linear motion-to-artefact transfer function [78].

The step size of an adaptive filter represents a compromise between the speed of adaptation and the noise in steady state. Various step sizes have been used to evaluate the PPG signal quality. The TVS-LMS algorithm offers rapid convergence. However, the AS-LMS algorithm provides not only rapid convergence, but also a minimal mean square error, as indicated by the high SNR value [79].

A simple and efficient approach based on the AS-LMS adaptive filter was applied to reduce motion artefacts in corrupted PPG signals [82].

A Laguerre series was implemented to represent the dynamics of walking and jogging using a few parameters, such as the HR. An adaptive blind-source separation technique was used to recover the physiological signal; however, this method has not yielded promising results to date [83].

In the absence of a triaxial accelerometer, singular value decomposition [88, 89], time and period domain analysis [90], adaptive comb filter (ACF) [91–93], spectrum subtraction [94], empirical mode decomposition (EMD) [95, 96], Wigner–Ville distribution [97], Kalman filtering [98–101], wavelet-based method [102–109], independent component analysis (ICA) [110–112], particle filter [113], and blind source separation [15, 16] can be used to generate a reference noise signal.

The number of motion artefacts differs according to the wavelength of light. The multichannel template-matching algorithm selects the channel with the least motion artefacts to calculate the PR for a particular time interval [114, 115].

Artefact corruption of the underlying photoplethysmographic signal was reduced in real time by an electronic processing methodology based on inversion of a physical artefact model. A heuristic physical model of motion artefacts was introduced and verified experimentally by inversion of a physical artefact model using an additional source-detector pair, resulting in a three-wavelength probe [116, 117]. In rPPG, a color filter array (CFA) is used to demosaicize and denoise the signal [118, 119]. The algorithm utilized signal decomposition and the support vector machine (SVM) model to remove motion artefacts from the PPG signal [110, 120–125]. Generally, the PPG signal and acceleration-derived features are extracted and classified using an SVM classifier.

The random forest method, which involves generation of a large number of classification trees, is also used for feature extraction. The random forest-based spectral peak-tracking algorithm identifies the spectral peak of the PR [126].

Deep and machine learning and neural networks have also been used to classify the PPG signal. However, methods based on neural networks and fuzzy systems require training or self-tuning of adaptive parameters [127–132]. For example, a combined ECG/PPG signal within a nonlinear system, based on a reaction–diffusion mathematical model implemented using the cellular neural network (CNN) methodology, was employed to filter the PPG signal by assigning a recognition score to the waveforms in the time series [132].

It is difficult to extract the pulse signals from a video signal because multiple wavelengths are used and there are noise artifacts. In a light-controlled environment, the extraction of PPG data based on analysis of RGB channels captured by a video camera has been successful. Under ambient illumination, however, many algorithmic image-processing techniques can be applied for single/multiple channel analysis to improve the extracted signal. The rPPG signal is strongly affected by noise artifacts, such as the subject's motions, facial expressions, talking, and variation in skin tone and illumination.

Camera imaging-based technologies can be divided into two categories: image photoplethysmography (iPPG) methods, which rely on the optical properties of skin color changes; and motion-based methods, which rely on the mechanical activity of the heart. A comprehensive review of remote monitoring technologies can be found elsewhere [133]. Detailed information can be obtained from Tables 3 and 4 in that paper [133]. In addition, the literature before 2104 was collected by the MIT rPPG imaging group [134].

In iPPG methods with ambient light, autoregressive (AR) spectral analysis is applied to extract the frequency bands of interest. For multiple channel analysis, PPG data are extracted and then FFT is applied to extract the frequency bands of interest [14]. Many algorithmic image-processing techniques based on the characteristics of the skin and wavelengths can be used with single/multiple channel analysis to improve the extracted signal [135].

Principle component analysis (PCA) and ICA are used for blind source separation, to distinguish skin pixels that contain PPG information and reduce the influence of variation in illumination [15, 16, 136, 137]. Chrominance (CHRO) signals are used to combine the color difference signals linearly by assuming standardized skin color to white-balance images [138].

The Eindhoven University group has proposed several new iPPG methods. The signature of the blood volume changes at different wavelengths was used to explicitly distinguish pulse-induced color changes from motion noise in RGB measurements [139]. Spatial subspace rotation was used to estimate the spatial subspace of skin pixels for pulse extraction and determined the temporal rotation in the image domain to extract the cardiac signal. The essential difference between these rPPG methods lies in the way that RGB signals are combined into a pulse-signal. A plane orthogonal to the skin was defined in the temporally normalized color space based on physiological reasoning [140–143].

Motion-based methods using a video camera are also commonly applied to measure pulse rate. Small amplitude motions in different regions of interest (ROIs) are captured.

2.5 Pulse-rate measurement and clinical trials

2.5.1 Pulse rate-measurement devices

Wearable PPG monitors are commonly used in healthcare, as well as in sports, to monitor the PR during periods of physical exertion. Such devices typically use green light and perform signal processing to reduce motion artefacts (see Sect. 2.4.4).

A large number of PR monitors are commercially available; however, their accuracy and validity are unclear. We assumed that most commercial devices calculated HR from PPG signals, but the algorithms are not known.

The Apple Watch, Basis Peak, Fitbit Surge, Microsoft Band, Mio Alpha 2, PulseOn, and Samsung Gear S2 were evaluated in terms of their ability to measure the HR while sitting, walking, running, and cycling; continuous HR telemetry was used as the gold standard for comparison [144] (Fig. 5).

HR measurements using commercially available devices typically have acceptable errors (<5%). These devices are regularly updated, and their algorithms tuned. Information on the precision of these devices is available on the Stanford University website [145].

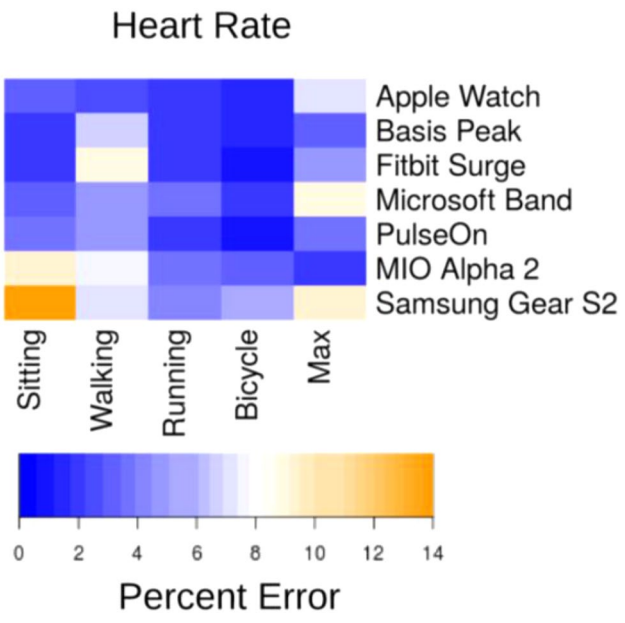

Fig. 5 Median device error. The acceptable error is<5% (dark colors); light colors indicate errors outside of this range. (A) Median error in heart rate (HR) by continuous HR telemetry

Daily use of commercial HR monitors has been the subject of validation studies [146–150], most of which involved the subjects performing predetermined activities. However, in the daily living monitor, Fitbit trackers either overestimated or underestimated the counts compared with the standard device. Therefore, their accuracy and sensitivity must be improved before they can be considered for monitoring of patients recommended to exercise by their physician [149].

The Fitbit Charge 2 [150] exhibited moderate bias on average, but showed poor precision for individual measurements, which could be underestimated by up to 30 bpm. The algorithm used by the Fitbit device to estimate HR is not widely used, and instability and improper positioning of the device may explain the variation in PR measurements. Standards for home use of commercially available HR monitors are needed, and the manufacturers should be required to validate the performance of their products in various settings.

2.5.2 Clinical trials and home use of cardiac monitors

Advances in wearable cardiac monitor technology are improving both the experience of the patient and the ability to analyze their cardiac activity. Previous cardiac-monitoring devices were hampered by low patient compliance and delayed access to data, but newer devices are less cumbersome and provide immediate access to data.

Healthcare management is important for preventing and predicting cardiac disease. Thus, the latest mobile and wearable devices can be used both in hospitals and in the community.

Mobile and wearable devices can monitor key physiological signals (*e.g.*, physical activity, HR, and PR and rhythm) to promote healthy behaviors, detect disease, and enable ongoing care. During physical activity, the PR can be accurately measured, but energy expenditure cannot. In this section, we describe the recent progress and challenges in monitoring the HR and rhythm for detection and management of artificial defibrillation (AF) [151].

Mobile and wearable devices for mobile health (mHealth) can be used to monitor the HR and heart rhythm of patients with cardiovascular disease. In particular, the detection and management of the most common type of arrhythmia—AF—enables prevention of strokes, management of symptoms, and reduction in the rate of hospitalization [152, 153].

Analysis of pulse data from a wrist-wearable device by novel algorithms can accurately detect the pulse irregularities associated with AF. The wrist-based wearables capable of pulse monitoring can be used over the long-term by patients with AF to enhance detection of paroxysmal AF and assessment of AF burden.

Several consumer-friendly, smartphone-connected handheld or wearable PPG monitors of the HR and heart rhythm from the finger, face, and wrist have been approved recently [144, 154, 155].

In fact, no specific standards must be followed or medical approval obtained for wearable physiological devices. The manufacturers of heart rate and pulse rate monitors do not have to obtain approval for their devices, and thus do not have to follow specific standards. However, most manufacturers follow the American National Standards Institute/Association for the Advancement of Medical Instrumentation (ANS/AAMI) EC13 standards. The disruption of EC13 2002 is used to acquire or display electrocardiographic signals with the primary purpose of continuous detection of cardiac rhythm. The accuracy criterion in the ANS/AAMI EC13:2002 (R2007) standard is a root mean square error (RMSE) ≤ 5 beats/min or $\leq 10\%$.

HR detection by the Cardiio smartphone application [156] was accurate at rest and after moderate- and vigorous-intensity exercise in healthy young adults. Contact-free facial PPG detection is more convenient but less accurate than finger PPG due to body movements after exercise [154]. Testing of contact PPGs (Instant Heart Rate ver. 3.0.1; Azumio, Palo Alto, CA, USA; and Heart Fitness ver. 2.0.3; Senscare SAS, France) and noncontact PPGs (What's My Heart Rate ver. 1.0; Vitrox Technologies, Malaysia; and Cardiio ver. 2.0; Cardiio, Cambridge, MA, USA) showed that the two contact photoplethysmography-based applications had superior feasibility and accuracy for HR measurement than the two non-contact photoplethysmography-based applications.

Measurement of the HR during rest and exercise by most wrist monitors is highly accurate [144, 157]. HR monitoring would be valuable to ensure that AF patients are adequately rate-controlled, to mitigate symptoms and decompensation [158, 159]. These technologies show promise for long-term noninvasive monitoring of AF.

However, a major concern regarding widespread use of AF-detection algorithms is lack of specificity, as other rhythms that create irregularity (*e.g.*, premature atrial or ventricular contractions, supraventricular tachycardia, and atrioventricular block) could be misclassified as AF. Artificial intelligence, neural networks, and machine learning have been applied to overcome this limitation of mHealth devices [160, 161].

Studies comparing Holter ECG and continuous pulse rates, using commercial software to determine R–R intervals and HR variability, have used a Markov model. Under the normalized absolute deviation (NAdev) and normalized absolute difference (NADiff), and the coefficient of the sample entropy features (COSen), AF detection was compared. With and without the Markov model, the specificities were 95, 89, 92, and 88%, respectively. As a result, the AI algorithm improved the specifications, comparable with the Food and Drug Administration-approved ECG-based AliveCor automated AF detector [159].

Wearable devices can also be used to monitor the PR of individuals undergoing cardiac rehabilitation [162] and for diabetes management [163].

In clinical practice, physicians tend to accept mobile and/or wearable devices that are simple to operate and inexpensive. Therefore, prior to their widespread clinical application, PPG devices require standardization in terms of their handling and accuracy at rest and during exercise.

3 Pulse oximetry

PPGs can be used for pulse oximetry; *i.e.*, for continuous noninvasive monitoring of the oxygen saturation of hemoglobin. Oxygen saturation is dependent on oxygen availability; *i.e.*, gas exchange in the lungs. Oxygen availability is an important parameter for evaluating gas exchange (oxygen and carbon dioxide), particularly during anesthesia and postoperatively. Oxygen saturation is typically expressed as a percentage rather than an absolute reading.

A pulse oximeter measures the oxygen saturation of arterial blood ($SpO_2\%$) noninvasively via a clip-like sensor attached to a fingertip. The $SpO_2\%$ is calculated from the amplitude of transmitted R and IR light, and the PR is determined from the PPG wave.

3.1 Principle of the pulse oximeter

Traditionally, the oxygen saturation of arterial blood was measured by drawing blood from an artery (*e.g.*, the radial or femoral artery) and subjecting it to blood-gas analysis. To measure oxygen saturation noninvasively, Dr. Takuo Aoyagi invented pulse oximetry in 1974 [164].

Hemoglobin can be divided into normal hemoglobin, which is capable of binding O_2, and dyshemoglobins, which are not. The normal hemoglobins include RHb and O_2Hb, while the dyshemoglobins include carboxyhemoglobin (COHb), methemoglobin (MetHb), and sulfhemoglobin (SHb) (Fig. 1). The total hemoglobin concentration (tHb) is expressed as:

$$\mathrm{tHb} = \mathrm{O_2Hb} + \mathrm{RHb} + \mathrm{Met\,Hb} + \mathrm{COHb} + \mathrm{SHb}$$

SHb is rare and can be omitted from the calculation. In normal circumstances, only oxygen-carrying hemoglobin is considered. Thus, the hemoglobin oxygen saturation, S, is:

$$\mathrm{S} = O_2\mathrm{Hb}/\left(\mathrm{O_2Hb} + \mathrm{RHb}\right)$$

The transmitted signal amplitude of arterial blood is measured using light at 660 nm (R) and 940 nm (IR).

The light absorption, A, of a blood sample is defined by the Beer-Lambert law as:

$$\mathrm{A} \equiv \log\left(\frac{I_0}{I}\right) = E \cdot C \cdot D \tag{1}$$

where I_0 is the incident light intensity, I is the transmitted light intensity, E is an extinction coefficient (dL/g/cm), C is the concentration (g/dL), and D is the thickness (cm).

The structure of the finger (Fig. 6) consists of tissue, venous blood, and arterial blood. The change in the systolic and diastolic phases in arterial blood is shown as the thickness, ΔD, of arterial blood. The transmitted light intensity difference between the systolic and diastolic phases (Fig. 6) is expressed in ΔI. Thus, the absorbance difference ΔA is expressed by the Lambert–Beer law as:

$$\Delta\mathrm{A} \equiv \log\frac{I}{I-\Delta I} = Eh \cdot Hb \cdot \Delta D \tag{2}$$

$$= \Delta\mathrm{I}/\left(\mathrm{I} - \frac{\Delta\mathrm{I}}{2}\right) = \frac{AC}{DC} \tag{3}$$

where Hb (g/dL) is the hemoglobin concentration, Eh (dL/g/cm) is the extinction coefficient of Hb, and ΔD (cm) is the change in the thickness of the arterial blood. At 660 and 940 nm, which are used for pulse oximeter measurements, the absorbance of other tissues in blood is ignored, except for oxy and deoxy Hb.

Using Eq. (2), the 660 nm (R) to 940 nm (R) light ratio is expressed as:

$$\emptyset = \frac{\Delta A_{660}}{\Delta A_{940}} = \frac{AC_{660}/DC_{660}}{AC_{940}/DC_{940}} \tag{4}$$

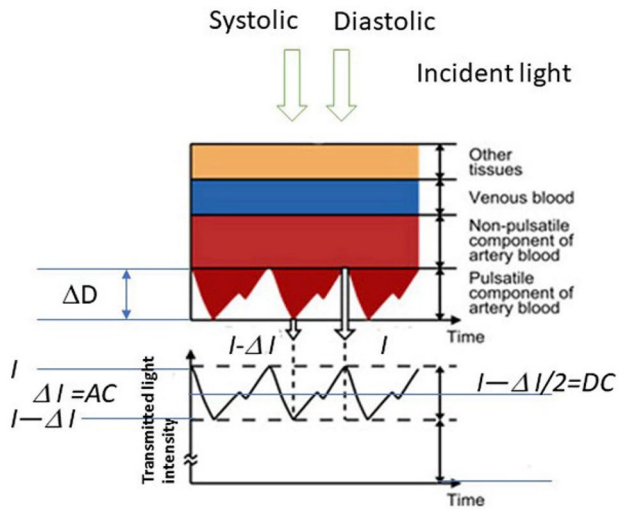

Fig. 6 Optical model of the fingertip

This equation clearly expresses the characteristic of the pulse oximeter, which measures arterial blood without considering variations in blood pulsation or hemoglobin concentration.

Eh, the extinction coefficient of tHb (RHb plus O_2Hb), can be calculated as the weighted average of Eo and Er, which corresponds to the concentration ratio:

$$\mathrm{Eh} = (\mathrm{Eo} \cdot \mathrm{S} + \mathrm{Er} \cdot (1 - \mathrm{S})) \tag{5}$$

Eo_{660}: Extinction coefficient of O_2Hb at 660 nm; Er_{660}: Extinction coefficient of RHb at 660 nm; Eo_{940}: Extinction coefficient of O_2Hb at 940 nm; Er_{940}: Extinction coefficient of RHb at 940 nm

where:

$$\mathrm{S} = \mathrm{O2Hb}/(\mathrm{O2Hb} + \mathrm{RHb})$$

$$\mathrm{O2Hb} + \mathrm{RHb} = 1$$

From Eqs. (4) and (5),

$$\boldsymbol{\Phi} \equiv \frac{\Delta A_{660}}{\Delta A_{940}} \cong \frac{\frac{AC_{660}}{DC_{660}}}{\frac{AC_{940}}{DC_{940}}} = \frac{Eo_{660} \cdot S + Er_{660} \cdot (1-S)}{Eo_{940} \cdot S + Er_{940} \cdot (1-S)} \tag{6}$$

where Eo_{660}, Er_{660}, Eo_{940}, and Er_{940} are constants. Then, ϕ is used to calibrate the standard curve according to S. Thus, we can calculate S from ϕ, which can be measured.

3.2 Electrical circuit

Figure 7 shows a block diagram of a typical pulse oximeter. Light at 660 and 940 nm transmitted through tissue is received by PDs, which measure the intensity of the two colors of pulse waves. The instrument next calculates the ΔA (= AC/DC) of the two colors of pulse waves to obtain ϕ, which is the ratio of ΔA between R and IR light, and converts ϕ to SpO_2.

The current signal of the PD is detected as a voltage and then converted to a digital signal by an A/D converter, with most of the processing being performed digitally. With the availability of high-speed AD converters, high-performance signal processors, and large memories, it has become possible to carry out logarithm calculations easily with a digital processor, as opposed to the approximate calculation of AC/DC in Eq. (2).

The current system-on-a-chip (SOC) technology has been applied to a simple AFE platform of pulse oximeter [165].

3.3 Portable and wearable pulse oximeters

The first portable pulse oximeter (ZB-831P) was developed by Nihon Kohden in 1994, and had a power consumption of only 15 mW. It can provide approximately 3 days of continuous monitoring with two AA alkaline battery cells, and

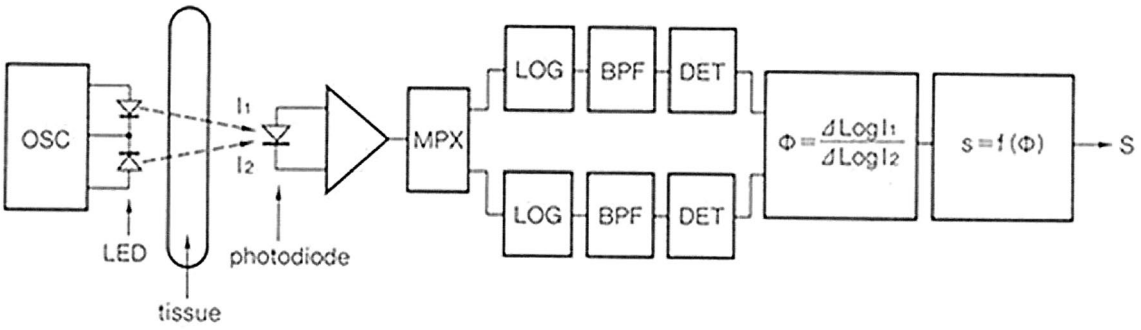

Fig. 7 Block diagram of a recent pulse oximeter

it satisfies the ISO 80601-2-61 standard for measurement accuracy.

The portable pulse oximeter has subsequently become even smaller. NONIN Medical (Minneapolis, MN, USA) released the world's first finger pulse oximeter, the Onyx 9500, in 1995. All components, measurement circuits, indicators, and batteries are contained in one unit that attaches to a fingertip. This product meets the measurement accuracy demanded of medical pulse oximeters in ISO 80601-2-61. It operates on two AAA alkaline batteries for approximately 1600 spot checks or up to 18 h of continuous operation.

A large number of fingertip-type oximeters are commercially available, but few meet the ISO 80601-2-61 measurement accuracy standards. Thus, we must use pulse oximeters very carefully. Examples of oxygen saturation meters that meet ISO are the MightySat and Pulsox (Fig. 7).

Several trials have examined watch-type oximeters with a finger senor. The watch is worn on the wrist and used as an interface instead of a standalone display device. Some wearable sensors are reflected types [166, 167]. A finger-free pulse oximeter was tested without wires or a fingertip probe. A reflective PPPG sensor was mounted on the bottom of the watchcase. The sensor consists of two or more LEDs and one or more PDs located side by side on the substrate (oCoare TM Pro 100, Taiwan Biophotonic, Taiwan) (Fig. 8).

3.4 Standards and accuracy

The ISO 80601-2-61 standards were established in 2011 to ensure the safety and basic operation of pulse oximeters. These standards require accuracy testing by a person, and the root mean square (rms) of the difference between the SpO_2 and SaO_2 measured from arterial blood must be less than 4% in the range of 70–100% SpO_2. The main factors that influence the accuracy are the LED wavelength, measurement site, signal strength, movement artefacts, and abnormal hemoglobin in the blood.

The difference in LED wavelengths greatly influences the value of ϕ in measurements. The fingertip is the most frequently used measurement site because it has a large number of capillaries; the forehead (using a reflectance sensor) and earlobe are also used. The influence of venous blood, the difference in optical passage between R and IR light, and the shunted light that reaches the detector without passing through blood-perfused tissues can cause measurement errors with reflectance sensors. If the earlobe is used, the patient's hands remain free [168–170].

Pulse oximeters measure the light transmitted from living tissue and calculate ΔA from the ratio of the DC component and the AC (pulsatile) component. The AC amplitude is much smaller than the DC amplitude, and the AC/DC ratio

Fig. 8 Wearable-type pulse oximeters. From left to right: MightySat™ Rx (Masimo), Onyx Vantage GO2 (Nonin), and Pulsox-310 (Konica Minolta)

is distributed between about 0.01% and 10%. The noise of the AC signal needs to be reduced if it is to be used for SpO_2 measurement.

Body movements, electric circuit noise, ambient light, and ambient electromagnetic noise can cause errors in SpO_2 measurements. Wearable sensors must be carefully attached to the body to reduce motion artefacts (see Sect. 2.4.4).

COHb and MeHb affect oxygen delivery to the tissues, and their levels can be measured using a multi-wavelength pulse oximeter. For example, the Radical7 pulse oximeter (Masimo) can measure SpO_2, COHb, and MetHb simultaneously using light of eight wavelengths. Most hemoglobin measuring devices measured the tHb, COHb and MeHb in the case of low perfusion [171–177]

With wearable pulse oximeters, there is little need to measure the levels of abnormal hemoglobins, but measurement of COHb is used to monitor carbon monoxide levels during firework displays.

3.5 Future perspectives

Oximeters are needed for oxygen management of patients receiving artificial respiration, surgery, or intensive care unit treatment, as well as for at-home oxygen management of respiratory diseases such as chronic obstructive pulmonary disease. Current wearable pulse oximeter designs are not satisfactory for performance of daily activities. Pulse oximeters incorporated in polysomnographs are used to diagnose sleep apnea syndrome (SAS) and hypoxemia. The use of pulse oximeters for at-home SAS screening would improve patient quality of life. In addition, morning surge can be estimated using a pulse oximeter, preferably a wearable one.

Such wearable pulse oximeters could even reduce the incidence of SAS by improving the rate of detection at low cost. This method would greatly contribute to public health and the medical device industry and would consequently be used widely. Confirmation that diseases can be prevented by daily measurement of blood oxygen saturation will promote the use of wearable pulse oximeters.

Pulse oximeters used for medical purposes outside of a hospital must meet the ISO 80601-2-61 accuracy standards. Several wearable oximeters that can be inaccurate are available, so users of such devices should first confirm their accuracy. The demand for high-end, medical-grade pulse oximeters remains, but new markets for cheaper, lower-end commoditized devices may appear in the future. Also, further applications of oximeters for home healthcare must be discussed.

4 Conclusion

The wearable PPG sensor and oximeter are popular devices for at-home healthcare and in the clinical setting, and can now be used to detect cardiovascular disease. Many challenges remain before the goal of effective mHealth interventions can be realized. Further work should focus on formulating scientific guidelines for proper handling of wearable PPG devices and establishing standards. Moreover, discussions among experts and regulatory bodies, funding agencies, and industry are needed to promote the development of accurate wearable devices.

Acknowledgements This study was supported in part by a Grant-in-Aid for Scientific Research (C) (Kakenhi) 17K01440 (2017–2019), METI project for promoting international standards (2018), and Japan Medical Research and Development Organization's (AMED) integrated Research and Development project for persons with disabilities (2017–2019).

Compliance with ethical standards

Conflict of interest The authors declare no conflict of interest.

Ethical statement In our review, our experiments have been approved by the institutional review board and the informed consents have been obtained from the human participants.

References

1. Hertzman AB. The blood supply of various skin areas as estimated by the photoelectric plethysmograph. Am J Physiol. 1938;124:328–40.
2. Challoner AVJ. Photoelectric plethysmography for estimating cutaneous blood flow. In: Rolfe P, editor. Non-invasive physiological measurement, vol. 1. Oxford: Academic Press; 1979. p. 127–51.
3. Kamal AAR, Harness JB, Irving G, Mearns AJ. Skin photoplethysmography—a review. Comput Methods Programs Biomed. 1989;28(4):257–69.
4. Alen J. Photoplethysmography and its application in clinical physiological measurement. Physiol Meas. 2007;28:R1–39.
5. Tamura T, Maeda Y, Sekine M, Yoshida M. Wearable photoplethysmographic sensors-past and present. Electronics. 2014;3(2):282–302.
6. Sun Y, Thakor N. Photoplethysmography revisited: from contact to noncontact, from point to imaging. IEEE Trans Biomed Eng. 2016;63(3):463–77.
7. Sami HM, Kleinman BS, Vassyl A, Lonchyna NA. Central venous pulsations associated with a falsely low oxygen saturation measured by pulse oximetry. J Clin Monit. 1991;7(4):309–12.
8. Shelley KH, Tamai D, Jablonka D, Gesquiere M, Stout RG, Silverman DG. The effect of venous pulsation on the forehead pulse oximeter wave form as a possible source of error in SpO_2 calculation. Anesth Analg. 2005;100:743–7.
9. Cui W, Ostrander LE, Lee BY. In vivo reflectance of blood and tissue as a function of light wavelength. IEEE Trans Biomed Eng. 1990;37(6):632–9.

10. Zijlstra WG, Buursma A, Meeuwsen-van der Roest WP. Absorption spectra of human fetal and adult oxyhemoglobin, de-oxyhemoglobin, carboxyhemoglobin, and methemoglibin. Clin Chem. 1991;37(9):1633–8.
11. Meada Y, Sekine M, Tamura T. The advantage of green reflected photoplethysmograph. J Med Syst. 2011;35(5):829–34.
12. Fallet S, Vesin JM. Robust heart rate estimation using wrist-type photoplethysmographic signals during physical exercise: an approach based on adaptive filtering. Physiol Meas. 2017;38:155–70.
13. Liao H-E. Two discrete oscillator based adaptive notch filters (OSC ANFs) for noisy sinusoids. IEEE Trans Signal Process. 2005;53:528–38.
14. Verkruysse W, Svaasand LO, Nelson JS. Remote plethysmographic imaging using ambient light. Opt Express. 2008;6(26):21434–45.
15. Poh MZ, McDuff DJ, Picard RW. Non-contact, automated cardiac pulse measurements using video imaging and blind source separation. Opt Express. 2010;18(10):10762–74.
16. Poh MZ, McDuff DJ, Picard RW. Advancements in noncontact, multiparameter physiological measurements using a webcam. IEEE Trans Biomed Eng. 2011;58(1):7–11.
17. Tarassenko L, Villarroel M, Guazzi A, Jorge J, Clifton DA, Pugh C. Non-contact video-based vital sign monitoring using ambient light and auto-regressive models. Physiol Meas. 2014;35:807–31.
18. Matsumura K, Rolfe P, Lee J, Yamakoshi T. iPhone 4s photoplethysmography: which light color yields the most accurate heart rate and normalized pulse volume using the iPhysioMeter application in the presence of motion artifact? PLoS ONE. 2014;9(3):e91205.
19. Spigulis J. Multispectral, fluorescent and photoplethysmographic imaging for remote skin assessment. Sensors (Basel). 2017;17(5):e1165.
20. Anderson RR, Parrish ED. The optics of human skin. J Invest Dermatol. 1981;77:13–9.
21. Bashkatov AN, Genina EA, Kochubey VI, Tuchin VV. Optical properties of human skin, subcutaneous and mucous tissues in the wavelength range from 400 to 2000 nm. J Phys D. 2005;38:2543–55.
22. Zhang Q, Styf JR, Gerdlé B, Lindberg LG. Non-invasive monitoring of muscle blood perfusion by photoplethysmography: evaluation of a new application. Acta Physiol Scand. 2005;183:335–43.
23. Sandberg M, Gailite L, Spigulis J, Lihachev A. Multilaser photoplethysmography technique. Lasers Med Sci. 2007;23:189–93.
24. Hagblad J, Lindberg LG, Andersson AK, Bergstrand S, Lindgren M, Ek AC, Folke M, Lindén M. A technique based on laser Doppler flowmetry and photoplethysmography for simultaneously monitoring blood flow at different tissue depths. Med Biol Eng Comput. 2010;48:415–22.
25. Kamshilin AA, Miridonov SV, Teplov VY, Saarenheimo R, Nippolainen E. Photoplethysmographic imaging of high spatial resolution. Biomed Opt Express. 2011;2:996–1006.
26. Jonathan E, Leahy M. Investigating a smartphone imaging unit for photoplethysmography. Physiol Meas. 2010;31(11):N79–83.
27. Jonathan E, Leahy MJ. Cellular phone-based photoplethysmographic imaging. J Biophotonics. 2011;4:293–6.
28. Scully CG, Lee J, Meyer J, Gorbach AM, Granquist-Fraser D, Mendelson Y, Chon KH. Physiological parameter monitoring from optical recordings with a mobile phone. IEEE Trans Biomed Eng. 2012;59:303–6.
29. Kamshilin AA, Nippolainen E, Sidorov IS, Vasilev PV, Erofeev NP, Podolian NP, Romashko RV. A new look at the essence of the imaging photoplethysmography. Sci Rep. 2015;5:1049.
30. Kamshilin AA, Mamontov OV, Koval VT, Zayats GA, Romashko RV. Influence of a skin status on the light interaction with dermis. Biomed Opt Express. 2015;6(11):4326–34.
31. Moço AV, Stuijk S, de Haan G. Skin inhomogeneity as a source of error in remote PPG-imaging. Biomed Opt Express. 2016;7(11):4718–33.
32. Moço AV, Stuijk S, de Haan G. New insights into the origin of remote PPG signals in visible light and infrared. Sci Rep. 2018;8(1):8501. https://doi.org/10.1038/s41598-018-26068-2.
33. Rhee S, Yang BH, Asada HH. Artifact-resistant, power-efficient design of finger-ring plethysmographic sensors. IEEE Trans Biomed Eng. 2001;48:795–805.
34. Jung JY, Lee LW. Zigbee device access control and reliable data transmission in Zigbee based health monitoring. In: Proc of 10th intern. conf. on advanced communication technology (ICACT 2008), vol 1; 2008. p. 795–7.
35. Lee Y, Shin H, Jo J, Lee Y. Development of a wristwatch-type PPG array sensor module. In: Proceedings of IEEE intern conf. on consumer electronics; 2011. p. 168–71.
36. Maguire M, Ward T. The design and clinical use of a reflective brachial photoplethysmograph. Technical report. Maynooth: National University of Ireland; 2002. p. 1–13.
37. Maeda Y, Sekine M, Tamura T. Relationship between measurement site and motion artifacts in wearable reflected photoplethysmography. J Med Syst. 2011;35(5):969–76.
38. Vogel S, Hülsbusch M, Henning T, Blazek V, Leonhardt S. In-ear vital signs monitoring using a novel microoptic reflective sensor. IEEE Trans Inf Technol Biomed. 2009;13(6):882–9.
39. Shin K, Kim Y, Bae S, Park K, Kim S. A novel headset with a transmissive PPG sensor for heart rate measurement. In: 13th International conference on biomedical engineering IFMBE proceedings, vol 23; 2009. p. 519–22.
40. Poh MZ, Swenson NC, Picard RW. Motion-tolerant magnetic earring sensor and wireless earpiece for wearable photoplethysmography. IEEE Trans Inf Technol Biomed. 2010;14(3):786–94.
41. Celka P, Verjus C, Vetter R. Motion resistant earphone located infrared based heart rate measurement device. In: Proc. 2nd int. conf. biomed. eng., Innsbruck; 2004. p. 582–5.
42. Poh MZ, Kim K, Goessling A, Swenson N, Picard R. Cardiovascular monitoring using earphones and a mobile device. Pervasive Comput. 2012;11(4):18–26.
43. Budidha K, Kyriacou PA. The human ear canal: investigation of its suitability for monitoring photoplethymographs and arterial oxygen saturation. Phys Meas. 2014;35(2):111–28.
44. Wang L, Lo B, Yang GZ. Multichannel reflective PPG earpiece sensor with passive motion cancellation. IEEE Trans Biomed Circuits Syst. 2007;1:235–41.
45. Wang CZ, Zheng YP. Home-telecare of the elderly living alone using a new designed ear-wearable sensor. In: 5th Int. workshop wearable implantable body sens. netw., Hong Kong; 2008. p. 71–4.
46. Patterson JAC, McIlwraith DG, Yang GZ. A flexible, low noise reflective PPG sensor platform for ear-worn heart rate monitoring. In: Proc. 6th int. workshop wearable implantable body sens. netw., Berkeley, CA; 2009. p. 286–91.
47. Kyriacou PA, Moye AR, Gregg RM, Choi DMA, Langford RM, Jones DP. A system for investigating oesophageal photoplethysmographic signals in anaesthetised patients. Med Biol Eng Comput. 1999;37(5):639–43.
48. Kyriacou PA, Powell S, Langford RM, Jones DP. Esophagel pulse oximetry utilizing reflectance photoplethysmography. IEEE Trans Biomed Eng. 2002;49(11):1360–8.
49. Kyriacou PA. Direct pulse oximetry within the esophagus, on the surface of abdominal viscera, and on free flaps. Anesth Analg. 2013;117(49):824–33.
50. Mendelson Y, Pujary C. Measurement site and photodetector size considerations in optimizing power consumption of a wearable reflectance pulse oximeter. In: Conference proceedings the IEEE eng med biol soc (EMBC 2003), vol 4; 2003. p. 3016–9.

51. Lee EM, Shin JY, Hong JH, Cha EJ, Lee TS. Glass-type wireless PPG measuring system. In: Conf. proc. IEEE eng med biol soc (EMBC2010), vol 1; 2010. p. 1433–6.
52. Reisner A, Shaltis PA, McCombie D, Asada HH. Utility of the photoplethysmogram in circulatory monitoring. Anesthesiology. 2008;108(5):950–8.
53. Teng XF, Zhang YT. The effect of contacting force on photoplethysmographic signals. Physiol Meas. 2004;25:1323–35.
54. Spigulis J. Optical non-invasive monitoring of skin blood pulsations. Appl Opt. 2005;44(10):1850–7.
55. Maeda Y, Sekine M, Tamura T, Mizutani K. The effect of contact pressure to the photoplethysmographic sensor during walking. In: Conf. procs eng med biol 2013 (EMBC 2013); 2013. p. R-307.
56. Dresher R. Wearable forehead pulse oximetry: minimization of motion and pressure artifacts. MS thesis. Worcester Polytechnic Institute; 2006. p. 1–83. https://web.wpi.edu/Pubs/ETD/Available/etd-050306-104212/unrestricted/Russ_Dresher_Thesis_53.pdf. Accessed 26 Dec 2018.
57. Dassel ACM, Graaff R, Sikkema M, Meijer A, Zijlstra WG, Aamoudse JG. Reflectance pulse oximetry at the forehead improves by pressure on the probe. J Clin Monit. 1995;11(4):237–44.
58. Dassel ACM, Graaff R, Meijer A, Zijlstra WG, Aarnoudse JG. Reflectance pulse oximetry at the forehead of newborns. The influence of varying pressure on the probe. J Clin Monit. 1996;12(6):421–8.
59. Dassel ACM, Graaff R, Aardema M, Zijlstra WG, Aarnoudse JG. Effect of location of the sensor on reflectance pulse oximetry. Br J Obstet Gynecol. 1997;104:910–6.
60. Hsiu H, Hsu CL, Wu TL. Effects of different contacting pressure on the transfer function between finger photoplethysmographic and radial blood pressure waveforms. J Eng Med. 2011;225(6):575–83.
61. Grabovskis A, Marcinkevics Z, Rubenis O, Rubinsa U, Lusab V. Photoplethysmography system for blood pulsation detection in unloaded artery conditions. Proc SPIE. 2012;8427:84270L.
62. Grabovskis A, Marcinkevics Z, Rubins U, Kviesis-Kipge E. Effect of probe contact pressure on the photoplethysmographic assessment of conduit artery stiffness. J Biomed Opt. 2013;18(2):027004. https://doi.org/10.1117/1.JBO.18.2.027004.
63. Sim JK, Ahn B, Doh I. A contact-force regulated photoplethysmography (PPG). AIP Adv. 2018;8:045210.
64. Liang Y, Elgendi M, Chen Z, Ward R. An optimal filter for short photoplethysmogram signals. Sci Data. 2018;5:180076. https://doi.org/10.1038/sdata.2018.76.
65. Lee HW, Lee JW, Jung WC, Lee GK. The periodic moving average filter for removing motion artifacts from PPG signals. Int J Control Autom Syst. 2007;5(6):701–6.
66. Lee J, Jung W, Kang IT, Kim Y, Lee G. Design of filter to reject motion artifact of pulse oximetry. Comput Stand Interfaces. 2004;26(39):241–9.
67. López-Silva SM, Giannetti R, Dotor ML. Heuristic algorithm for photoplethysmographic heart rate tracking during maximal exercise test. J Med Biol Eng. 2012;32:181–8.
68. Reddy KA, George B, Kumar VJ. Use of Fourier series analysis for motion artifact reduction and data compression of photoplethysmographic signals. IEEE Trans Instrum Meas. 2009;58(5):1706–11.
69. Dubey H, Kumaresan R, Mankodiya KJ. Harmonic sum-based method for heart rate estimation using PPG signals affected with motion artifacts. Ambient Intell Human Comput. 2018;9:137–50. https://doi.org/10.1007/s12652-016-0422-z.
70. Graybeal JM, Petterson MT. Adaptive filtering and alternative calculations revolutionizes pulse oximetry sensitivity and specificity during motion and low perfusion. Eng Med Biol Soc. 2004;2:5363–6.
71. Asada HH, Jiang HH, Gibbs P. Active noise cancellation using MEMS accelerometers for motion-tolerant wearable bio-sensors. In: Conf. proc. IEEE eng med biol. soc., vol 3; 2004. p. 2157–60.
72. Gibbs PT, Wood LB, Asada HH. Active motion artifact cancellation for wearable health monitoring sensors using collocared MEMS accelerometers. In: Proc. SPIE5765, smart structures and materials 2005: sensors and smart structures technologies for civil, mechanical, and aerospace systems; 2005. p. 811. https://doi.org/10.1117/12.600781.
73. Yousefi R, Nourani M, Ostadabbas S. A motion-tolerant adaptive algorithm for wearable photoplethysmographic biosensors. IEEE J Biomed Health Inf. 2014;18:670–81.
74. Alzahrani A, Hu S, Azorin-Peris V. A comparative study of physiological monitoring with a wearable opto-electronic patch sensor (OEPS) for motion reduction. Biosensors. 2015;5(2):288–307. https://doi.org/10.3390/bios5020288.
75. Han H, Kim M-J, Kim J. Development of real-time motion artifact reduction algorithm for a wearable photoplethysmography. In: Conf. proc. IEEE eng. med. biol. soc., vol 3; 2007. p. 1538–41.
76. Han H, Kim J. Artifacts in wearable photoplethysmographs during daily life motions and their reduction with least mean square based active noise cancellation method. Comput Biol Med. 2012;42:387–93.
77. Chan KW, Zhang YT. Adaptive reduction of motion artifact from photoplethysmographic recordings using a variable step size LMS filter. Proc IEEE Sens. 2002;2002(2):1343–6.
78. Wei P, Guo R, Zhang J, Zhang YT. A new wristband wearable sensor using adaptive reduction filter to reduce motion artifact. In: Conf prof IEEE ITAB 2008; 2008. p. 278–9.
79. Ram MR, Madhav KV, Krishna EH, Reddy KN, Reddy KA. On the performance of time varying step-size least mean squares (TVS-LMS) adaptive filter for MA reduction from PPG signals. In: International conference on communications and signal processing (ICCSP); 2011. p. 1–8.
80. Park C, Shin H, Lee B. Blockwise PPG enhancement based on time-variant zero-phase harmonic notch filtering. Sensors (Basel). 2017;17(4):860. https://doi.org/10.3390/s17040860.
81. Salehizadeh SMA, Dao D, Bolkhovsky J, Cho C, Mendelson Y, Chon KH. A novel time-varying spectral filtering algorithm for reconstruction of motion artifact corrupted heart rate signals during intense physical activities using a wearable photoplethysmogram sensor. Sensors. 2016;16(2):10.
82. Ram MR, Madhav KV, Krishna EH, Komalla NR, Reddy KA. A novel approach for artifact reduction in PPG signals based on AS-LMS adaptive filter. IEEE Instrum Meas. 2012;61(5):1445–57.
83. Widraw B, Glover JR Jr, McCool JM Jr, Kaunitz J, Williams CS, Hearn RH, Zeidler JR, Dong E Jr, Goodlin RC. Adaptive noise cancellation: principles and applications. Proc IEEE. 1975;63(12):1692–716.
84. Wood LB, Asada HH. Noise cancellation model validation for reduced motion artifact wearable PPG sensors using MEMS accelerometers. In: Conference proceedings IEEE EMBS 2006; 2006. p. 3525–8
85. Wood LB, Asada HH. Low variance adaptive filter for cancelling motion artifact in wearable photoplethysmogram sensor signals. In: Conference proceedings IEEE EMBS 2007; 2007. p. 652–5.
86. Wood LB, Asada HH. Active motion artifact reduction for wearable sensors using Laguerre expansion and signal separation. In: Conference proceedings IEEE EMBS 2005; 2005. p. 652–5.
87. Wood LB. Motion artifact reduction for wearable photoplethysmogram sensors using micro accelerometers and Laguerre series adaptive filters. MIT MS Thesis; 2008. p. 1–74.
88. Reddy KA, Kumar VJ. Motion artifact reduction in photoplethysmographic signals using singular value decomposition. In: Proceedings of the 2007 IEEE instrumentation and measurement

technology conference, Warsaw; 2007. https://doi.org/10.1109/imtc.2007.379467.
89. Rojano JF, Isaza CV. Singular value decomposition of the Time-Frequency distribution of PPG signals for motion artifact reduction. Int J Signal Process Syst. 2016;4(6):475–82.
90. Couceiro R, Carvalho P, Paiva RP. Detection of motion artifact patterns in photoplethysmographic signals based on time and period domain analysis. Physiol Meas. 2014;35:2369–88.
91. Nehorai A, Porat B. Adaptive comb filtering for harmonic signal enhancement. IEEE Trans Acoust Speech Signal Proc. 1986;34(5):1124–38.
92. Lee B, Kee Y, Han J, Yi WJ. Adaptive comb filtering for motion artifact reduction from PPG with a structure of adaptive lattice IIR notch filter. In: Conference proc. of EMBC2011; 2011. p. 7937–40.
93. Kim SC, Hwang EJ, Kim DW. Noise reduction of PPG signal during free movements using adaptive SFLC (scaled Fourier liner combiner). IFMBE Proc. 2007;14:1191–4.
94. Zhang Y, Liu B, Zhang Z. Combining ensemble empirical mode decomposition with spectrum subtraction technique for heart rate monitoring using wrist-type photoplethysmography. Biomed Signal Process Control. 2015;21:119–25.
95. Sun X, Yang P, Li Y, Gao Z, Zhang YT. Robust heart beat detection from photoplethysmography interlaced with motion artifacts based on empirical mode decomposition. In: Proceedings of the 2012 IEEE-EMBS international conference on biomedical and health informatics (BHI); 2012. p. 775–8.
96. Fukushima H, Kawanaka H, Bhuiyan MS. Estimating heart rate using wrist-type photoplethysmography and acceleration sensor while running. In: Proceedings of the 2012 annual international conference of the IEEE engineering in medicine and biology society (EMBC); 2012. p. 2901–4.
97. Yan YS, Poon CC, Zhang YT. Reduction of motion artifact in pulse oximetry by smoothed pseudo Wigner-Ville distribution. J Neuroeng Rehab. 2005;2:1–9.
98. Lee SM, Zhang YT. Reduction of motion artifacts from photoplethysmographic recordings using a wavelet denoising approach. In: Proc. IEEE Asian-Pacific conference EMBS; 2003. p. 194–5.
99. Seyeditabaii S, Seyedtabaii L. Kalman filter based adaptive reduction of motion artifact from photoplethysmographic signal. In: Proc. World Academy of Science, Engineering and Technology, vol 39; 2008. p. 173–6.
100. Lee B, Han J, Baek HJ, Shin JH, Park KW, Yi WJ. Improved estimation of motion artifacts from a photoplethysmographic signal using a Kalman smoother with simultaneous accelerometry. Physiol Meas. 2010;31:1585–603.
101. Foussier J, Teichmann D, Jia J, Misgeld B, Leonhardt S. An adaptive Kalman filter approach for cardiorespiratory signal extraction and fusion of non-contacting sensors. BMC Med Inf Decis Mak. 2014;14:37. https://doi.org/10.1186/1472-6947-14-37.
102. Lee S, Ibey BL, Xu W, Wilson MA, Ericson MN, Coté GL. Processing of pulse oximeter data using discrete wavelet analysis. IEEE Trans Biomed Eng. 2005;52(7):1350–2.
103. Foo JYA. Comparison of wavelet transformation and adaptive filtering in restoring artifact-induced time-related measurement. Biomed Signal Process Control. 2006;1(1):93–8.
104. Fu TH, Liu SH, Tang KT. Heart rate extraction from photoplethysmogram waveform using wavelet multi-resolution analysis. J Med Biol Eng. 2008;20(4):229–32.
105. Foo JYA. Use of independent component analysis to reduce motion artifact in pulse transit time measurement. IEEE Signal Process Lett. 2008;15:124–6.
106. Raghuram M, Madhav KV, Krishna EH, Reddy KA. On the performance of wavelets in reducing motion artifacts from photoplethysmographic signals. In: 2010 4th international conference on bioinformatics and biomedical engineering; 2010. https://doi.org/10.1109/icbbe.2010.5516291.
107. Raghuram M, Madhav KV, Krishna EH, Komalla N, Sivani RK, Reddy KA. Dual-tree complex wavelet transform for motion artifact reduction of PPG signals. In: 2012 IEEE international symposium on medical measurements and applications proceedings; 2012. p. 39–42. https://doi.org/10.1109/memea.2012.6226643.
108. Bai T, Li D, Wang H, Pang Y, Li G, Lin J, Zhou Q, Jeon G. A PPG signal de-noising method based on the DTCWT and the morphological filtering. In: 2016 12th International conference on signal-image technology & Internet-based systems (SITIS); 2016. p. 503–6.
109. Dao D, Salehizadeh SMA, Noh Y, Chong JW, Cho CH, McManus D, Darling CE, Mendelson Y, Chon KH. A robust motion artifact detection algorithm for accurate detection of heart rates from photoplethysmographic signals using time-frequency spectral features IEEE J Biomed Health Infom. 2017;21(5):1242–53.
110. Yao J, Warren S. A short study to assess the potential of independent component analysis for motion artifact separation in wearable pulse oximeter signals. In: Conf Proc. IEEE EMBS2005; 2005. p. 3585–8.
111. Kim BS, Yoo SK. Motion artifact reduction in photoplethysmography using independent component analysis. IEEE Trans Biomed Eng. 2006;53:566–8.
112. Peng F, Zhang Z, Gou X, Liu H, Wang W. Motion artifact removal from photoplethysmographic signals by combining temporally constrained independent component analysis and adaptive filter. Biomed Eng OnLine. 2014;13:50. https://doi.org/10.1186/1475-925X-13-50.
113. Lee Y-K, Jo J, Lee Y, Shin H-S, Kwon O-W. Particle filter-based noise reduction of PPG signals for robust emotion recognition. In: Proc. IEEE consumer electronics (ICCE); 2012. p. 598–9.
114. Li Q, Clifford GD. Dynamic time warping and machine learning for signal quality assessment of pulsatile signals. Physiol Meas. 2012;33(9):1491–502.
115. Warren KM, Harvey JR, Chon KH, Mendelson Y. Improving pulse rate measurements during random motion using a wearable multichannel reflectance photoplethysmograph. Sensors (Basel, Switzerland). 2016;16(3):342. https://doi.org/10.3390/s16030342.
116. Hayes MJ, Smith PR. Artifact reduction in photoplethysmography. Appl Opt. 1998;37(31):7437–46.
117. Hayes MJ, Smith PRA. New method for pulse oximetry processing inherent insensitivity to artifact. IEEE Trans Biomed Eng. 2001;48(4):452–61.
118. Bosco A, Battiato S, Bruna A, Rizzo R. Noise reduction for CFA image sensors exploiting HVS behaviour. Sensors (Basel, Switzerland). 2009;9(3):1692–713. https://doi.org/10.3390/s90301692.
119. Lee MS, Park SW, Kang MG. Denoising algorithm for CFA image sensors considering inter-channel correlation. Sensors. 2017;17:1236.
120. Lai PH, Kim I. Lightweight wrist photoplethysmography for heavy exercise: motion robust heart rate monitoring algorithm. Health Technol Lett. 2015;2:6.
121. Chong JW, Dao DK, Salehizadeh SMA, McManus DD, Darling CE, Chon KH, Mendelson Y. Photoplethysmograph signal reconstruction based on a novel hybrid motion artifact detection–reduction approach. Part I: motion and noise artifact detection. Ann Biomed Eng. 2014;42(11):2238–50.
122. Zhang Z, Pi Z, Liu B. TROIKA: a general framework for heart rate monitoring using wrist-type photoplethysmographic signals during intensive physical exercise. IEEE Trans Biomed Eng. 2014;62:522–31.

123. Zhang Z. Photoplethysmography-based heart rate monitoring in physical activities via joint sparse spectrum reconstruction. IEEE Trans Biomed Eng. 2015;62:1902–10.
124. Xiong J, Cai L, Wang F, He X. SVM-based spectral analysis for heart rate from multi-channel WPPG sensor signals. Sensors (Basel). 2017;17(3):E506.
125. Reljin N, Zimmer G, Malyuta Y, Shelley K, Mendelson Y, Blehar DJ, Darling CE, Chon KH. Using support vector machines on photoplethysmographic signals to discriminate between hypovolemia and euvolemia. PLoS ONE. 2018;13(3):e0195087. https://doi.org/10.1371/journal.pone.0195087.
126. Ye Y, He W, Cheng Y, Huang W, Zhang Z. A robust random forest-based approach for heart rate monitoring using photoplethysmography signal contaminated by intense motion artifacts. Sensors (Basel). 2017;17(2):38. https://doi.org/10.3390/s17020385.
127. Soltane M, Ismail M, Abidin Z, Rashid A. Artificial neural networks (ANN) approach to PGG signal classification. Int J Comput Inf Sci. 2004;2(1):58–65.
128. Kurylyak Y, Lamonaca F, Grimaldi D. A neural network-based method for continuous blood pressure estimation from a PPG signal. In: 2013 IEEE international instrumentation and measurement technology conference (I2MTC); 2013. p. 200–3.
129. Jindal V, Birjandtalab J, Pouyan MB, Nourani M. An adaptive deep learning approach for PPG-based identification. In: 2016 38th Annual international conference of the IEEE engineering in medicine and biology society (EMBC); 2016. p. 6401–4.
130. Tarvirdizadeh B, Golgouneh A, Tajdari F, Khodabakhshi E. A novel online method for identifying motion artifact and photoplethysmography signal reconstruction using artificial neural networks and adaptive neuro-fuzzy inference system. Neural Comput Appl. 2018. https://doi.org/10.1007/s00521-018-3767-8.
131. Du Y-C, Stephanus A. Levenberg-Marquardt neural network algorithm for degree of arteriovenous fistula stenosis classification using a dual optical photoplethysmography sensor. Sensors (Basel, Switzerland). 2018;18(7):2322. https://doi.org/10.3390/s18072322.
132. Rundo F, Conoci S, Ortis A, Battiato S. An advanced bio-inspired photoplethysmography (PPG) and ECG pattern recognition system for medical assessment. Sensors (Basel, Switzerland). 2018;18(2):405. https://doi.org/10.3390/s18020405.
133. Alnaji A, Gibson K, Lee SH, Chahl J. Monitoring of cardiorespiratory signal: principles of remote measurements and review of methods. IEEE Access. 2017;5:15776–90.
134. Remote photoplethysmographic (PPG) imaging using digital cameras. http://alumni.media.mit.edu/~djmcduff/assets/remote-physiology.html#literature. Accessed 20 Dec 2018.
135. Feng L, Po LM, Xu X, Li Y, Ma R. Motion-resistant remote imaging photoplethysmography based on the optical properties of skin. IEEE Trans Circuits Syst Video Technol. 2015;25(5):879–91.
136. Qi H, Guo Z, Chen X, Shen Z, Wang ZJ. Video-based human heart rate measurement using joint blind source separation. Biomed Signal Process Control. 2017;31:309–20.
137. Lewandowska M, Rumiski J, Kocejko T, Nowak J. Measuring pulse rate with a webcam—a non-contact method for evaluating cardiac activity. In Proc. federated conf. comput. sci. inf. syst.; 2011. p. 405–10.
138. de Haan G, Jeanne V. Robust pulse rate from chrominance-based rPPG. IEEE Trans Biomed Eng. 2013;60(10):2878–86.
139. de Haan G, van Leest A. Improved motion robustness of remote PPG by using the blood volume pulse signature. Physiol Meas. 2014;35(9):1913–26.
140. Wang W, Stuijk S, de Haan G. A novel algorithm for remote photoplethysmography: spatial subspace rotation. IEEE Trans Biomed Eng. 2016;63(9):1974–84.
141. Wang W, den Brinker A, Stuijk S, de Haan G. Algorithmic principles of remote PPG. IEEE Trans Biomed Eng. 2017;64(7):1479–91.
142. Wang W, Stuijk S, de Haan G. Living-skin classification via remote-PPG. IEEE Trans Biomed Eng. 2017;64(12):2781–92.
143. Wang W, den Brinker AC, de Haan G. Full video pulse extraction. Biomed Opt Express. 2018;9:3898–914.
144. Shcherbina A, Mattsson CM, Waggott D, Salisbury H, Christle JW, Hastie T, Wheeler MT, Ashley EA. Accuracy in wrist-worn, sensor-based measurements of heart rate and energy expenditure in a diverse cohort. J Pers Med. 2017;7(2):E3.
145. Ashley Lab Protocol—Device Validation Datahub—Stanford University https://ashleylab.stanford.edu/science/digital-health. Accessed 20 Oct 2018.
146. Sartor F, Papini G, Cox LGE, Cleland J. Methodological shortcomings of wrist-worn heart rate monitors validations. J Med Internet Res. 2018;20(7):e10108.
147. Hernando D, Roca S, Sancho J, Alesanco Á, Bailón R. Validation of the apple watch for heart rate variability measurements during relax and mental stress in healthy subjects. Sensors. 2018;18:2619.
148. Thiebaud RS, Funk MD, Patton JC, Massey BL, Shay TE, Schmidt MG, Giovannitti N. Validity of wrist-worn consumer products to measure heart rate and energy expenditure. Digit Health. 2018;4:2055207618770322. https://doi.org/10.1177/2055207618770322.
149. Gorny AW, Liew SJ, Tan CS, Müller-Riemenschneider F. Fitbit charge HR wireless heart rate monitor: validation study conducted under free-living conditions. JMIR Mhealth Uhealth. 2017;5(10):e157.
150. Benedetto S, Caldato C, Bazzan E, Greenwood DC, Pensabene V, Actis P. Assessment of the Fitbit Charge 2 for monitoring heart rate. PLoS ONE. 2018;13(2):e0192691.
151. McConnell MV, Turakhia MP, Harrington RA, King AC, Ashley EA. Mobile health advances in physical activity, fitness, and atrial fibrillation. J Am Coll Cardiol. 2018;71(23):2691–701. https://doi.org/10.1016/j.jacc.2018.04.030.
152. Noah B, Keller MS, Mosadeghi S, Spiegel BMR. Impact of remote patient monitoring on clinical outcomes: an updated meta-analysis of randomized controlled trials. NPJ Digit Med. 2018;1:2.
153. Turakhia MP, Kaiser DW. Transforming the care of atrial fibrillation with mobile health. J Interv Card Electrophysiol. 2016;47:45–50.
154. Yan BP, Chan CK, Li CK, To OT, Lai WH, Tse G, Poh YC, Poh MZ. Resting and postexercise heart rate detection from fingertip and facial photoplethysmography using a smartphone camera: a validation study. JMIR Mhealth Uhealth. 2017;5:e33.
155. Coppetti T, Brauchlin A, Müggler S, Attinger-Toller A, Templin C, Schönrath F, Hellermann J, Lüscher TF, Biaggi P, Wyss CA. Accuracy of smartphone apps for heart rate measurement. Eur J Prev Cardiol. 2017;24:1287–93.
156. Cardiio https://www.cardiio.com/. Accessed 20 Oct 2018.
157. Wang R, Blackburn G, Desai M, Phelan D, Gillinov L, Houghtaling P, Gillinov M. Accuracy of wrist-worn heart rate monitors. JAMA Cardiol. 2017;2:104–6.
158. Chan P, Wong C, Poh YC, Pun L, Leung WW, Wong YF, Wong MM, Poh MZ, Chu DW, Siu CW. Diagnostic performance of a smartphone-based photoplethysmographic application for atrial fibrillation screening in a primary care setting. J Am Heart Assoc. 2016;5:e003428.
159. Bonomi AG, Schipper F, Eerikäinen LM, Margarito J, van Dinther R, Muesch G, Morree HM, Aarts RM, Babaeizadeh S, McManus DD, Dekker LRC. Atrial fibrillation detection using a novel cardiac ambulatory monitor based on photo-plethysmography at the wrist. J Am Heart Assoc. 2018;7:e009351.

160. Krittanawong C, Zhang H, Wang Z, Aydar M, Kitai T. Artificial intelligence in precision cardiovascular medicine. J Am Coll Cardiol. 2017;69:2657–64.
161. Yousefi ZR, Parak J, Tarniceriu A, Harju J, Yli-Hankala A, Korhonen I, Vehkaoja A. Atrial fibrillation detection from wrist photoplethysmography data using artificial neural networks. In: Lhotska L, Sukupova L, Lacković I, Ibbott G (eds) World congress on medical physics and biomedical engineering 2018. IFMBE Proceedings, vol 68/2. Singapore: Springer; 2019.
162. Medina Quero J, Fernández Olmo MR, Peláez Aguilera MD, Espinilla Estévez M. Real-time monitoring in home-based cardiac rehabilitation using wrist-worn heart rate devices. Sensors. 2017;17:2892.
163. Yavelberg L, Zaharieva D, Cinar A, Riddell MC, Jamnik V. A pilot study validating select research-grade and consumer-based wearables throughout a range of dynamic exercise intensities in persons with and without type 1 diabetes: a novel approach. J Diabetes Sci Technol. 2018;12(3):569–76.
164. Aoyagi T, Kishi M, Yamaguchi K, Watanabe S. Improvement of the earpiece oximeter. Japanese Society of Medical Electronics and Biological Engineering; 1974. p. 90–1.
165. Glaros KN, Drakakis EM. A sub-mW fully-integrated pulse oximeter front-end. IEEE Trans Biomed Circuits Syst. 2013;7(3):363–75.
166. Lee H, Ko H, Lee J. Reflectance pulse oximetry: practical issues and limitations. ICT Express. 2016;2(4):195–8.
167. Baek HJ, Shin JW, Cho J. The effect of optical crosstalk on accuracy of reflectance type pulse oximeter for mobile healthcare. J Healthc Eng; 2018. Article ID 3521738.
168. Agashe GS, Coakley J, Mannheimer PD. Forehead pulse oximetry: headband use helps alleviate false low readings likely related to venous pulsation artifact. Anesthesiology. 2006;105(6):1111–6.
169. Mannheimer PD. The light-tissue interaction of pulse oximetry—review. Anesth Analg. 2007;105(6 Suppl):S10–7.
170. Patterson JAC, Yang GZ. Ratiometric artifact reduction in low power reflective photoplethysmography. IEEE Trans Biomed Circuits Syst. 2011;5(4):330–8.
171. Nitzan M, Romem A, Koppel R. Pulse oximetry: fundamentals and technology update. Med Devices (Auckland, NZ). 2014;7:231–9. https://doi.org/10.2147/MDER.S47319.
172. Reynolds KJ, Palayiwa E, Moyle JT, Sykes MK, Hahn CE. The effect of dyshemoglobins on pulse oximetry: part I, theoretical approach and part II, experimental results using an in vitro test system. J Clin Monit. 1993;9(2):81–90.
173. Barker SJ, Badal JJ. The measurement of dyshemoglobins and total hemoglobin by pulse oximetry. Curr Opin Anaesthesiol. 2008;21(6):805–10.
174. Shamir MY, Avramovich A, Smaka T. The current status of continuous noninvasive measurement of total, carboxy, and methemoglobin concentration. Anesth Analg. 2012;114:972–8.
175. Baulig W, Seifert B, Spahn DR, Theusinger OM. Accuracy of non-invasive continuous total hemoglobin measurement by pulse CO-oximetry in severe traumatized and surgical bleeding patients. J Clin Monit Comput. 2017;31:177–85. https://doi.org/10.1007/s10877-015-9816-2.
176. Louie A, Feiner JR, Bicker PE, Rhodes L, Bernstein M, Lucero J. Four types of pulse oximeters accurately detect hypoxia low perfusion and motion. Anesthesiology. 2018;128:520–30.
177. Murphy SM, Omar S. The clinical utility of noninvasive pulse co-oximetry hemoglobin measurements in dark-skinned critically ill patients. Anesth Analg. 2018;126(5):1519–26.